CENTRAL RAPIDITY DENSITIES OF CHARGED PARTICLES AT RHIC AND LHC

N. Armesto*

Departamento de Física, Módulo C2, Planta baja, Campus de Rabanales,

Universidad de Córdoba, E-14071 Córdoba, Spain

and

C. Pajares†

Departamento de Física de Partículas, Universidade de Santiago de Compostela,

E-15706 Santiago de Compostela, Spain

February 2000

Abstract

Predictions on central rapidity densities of charged particles at energies of the Relativistic Heavy Ion Collider and the Large Hadron Collider, for central collisions between the largest nuclei that will be available at these accelerators, are reviewed. Differences among the results of the existing models are discussed in relation with their underlying physical basis and with the possibilities to discriminate them.

US-FT/2-00

UCOFIS 1/00

hep-ph/0002163

*E-mail: fa1arpen@uco.es.

†E-mail: pajares@gaes.usc.es.

1 Introduction

In the last years many experimental and theoretical efforts have been devoted to search Quark Gluon Plasma (QGP) and/or collective effects[1] in heavy ion collisions [1, 2, 3, 4, 5, 6], as a tool to study the nonperturbative aspects of Quantum Chromodynamics (QCD). To achieve this goal several signatures of the phase transition(s) from confined to deconfined quarks and gluons and of chiral symmetry restoration have been proposed.

The finding of three of the proposed [7, 8, 9] signals at the Super Proton Synchrotron (SPS) at CERN has originated great excitement and debate in the scientific community in this field. In fact, an abnormal suppression of J/ψ [10] and a strong enhancement of strange baryons and antibaryons [11] have been observed in central[2] Pb-Pb collisions, compared with those measured in collisions between lighter projectiles and targets. Also an enhancement in the dilepton spectrum for dilepton masses below 0.8 GeV/c^2 has been seen in Pb-Au collisions [12]. Whether or not these three experimental observations are really an unambiguous proof of the existence of a QGP is still an open question [13, 14, 15, 16, 17, 18, 19, 20, 21], due to their possible explanation using more conventional, but still interesting, physics. In any case, it is expected that the forthcoming heavy ion experiments in the Relativistic Heavy Ion Collider (RHIC) at BNL and the Large Hadron Collider (LHC) at CERN will clarify definitively the point[3] .

In spite of the work done these last years there are many fundamental aspects of the physics of heavy ions at high energies which are not clear at all. Fundamental questions like, e.g.:

- Is particle rapidity density proportional to the number of participant nucleons or to the number of elementary nucleon-nucleon collisions?
- Which is the physical explanation of the SPS particle correlation data?
- How large will particle multiplicities be at RHIC and LHC?

are answered in a very different way by several models, all of them claiming to agree with the existing experimental data.

[1] Collective effects are those considered to explain the event, which go beyond the superposition of elementary nucleon-nucleon collisions.

[2] By central collision we mean a head-on one, in which most of the matter of the lightest nucleus participates. In practice different criteria are used, both theoretically (upper bound in impact parameter, minimum number of participant wounded nucleons,...) and experimentally (percentage of the cross section, lower bound in the number of charged particles,...).

[3] RHIC and LHC will provide center of mass energies of 200 GeV and 5.5 TeV per nucleon respectively, to be compared with $\sim$ 20 GeV per nucleon at the SPS.

Referring to the last question, in Fig. 1 it is shown the pseudorapidity distribution of charged particles from different models for central Pb-Pb collisions at a beam energy of 3 TeV per nucleon; this plot has been taken from the ALICE[4] Technical Proposal [22] done by the ALICE Event Generator Pool in December 1995. The results according to Monte Carlo codes of several models show large differences at central pseudorapidity. Indeed, between the String Fusion Model (SFM) [23] and the VENUS [24] or SHAKER [25] codes there is a factor larger than 4 at $\eta = 0$, while the difference in the fragmentation regions ($|\eta| \geq 5$) is smaller. At RHIC energy[5] the difference is about a factor 2 - most models give results in the range $700 \div 1500$.

These uncertainties in one of the most elementary aspects of the collision, may leave us uncomfortable regarding the necessity to keep under control the conventional physics of heavy ions to clearly distinguish the signatures of QGP and/or collective effects in the proposed observables. Needless to say, from the experimental point of view it is crucial to know whether there will be 2000 or 8000 charged particles per unit rapidity in central Pb-Pb collisions at the LHC for the design of the detectors. For these reasons we review in this paper charged particle central rapidity density predictions of different models for central collisions between the largest nuclei that will be available at RHIC and LHC, discussing the origin of the differences among the results.

According to their origin, models can be classified into three categories. On the one hand, some models like Dual Parton Model (DPM) [27, 28, 29], its Monte Carlo implementation DPMJET [30, 31], Quark-Gluon String Model (QGSM) [32], FRITIOF [33], SFM [23, 34, 35], Relativistic Quantum Molecular Dynamics (RQMD) [36, 37, 38], Ultrarelativistic Quantum Molecular Dynamics (UrQMD) [39, 40], VENUS [24] or its new version NEXUS [41], and LUCIAE [42] mainly pay attention to the soft part of the collision (there is no need of a hard perturbative part at SPS energies). The hard part in some of these models is included adding to the elementary soft cross section the jet one, as an input for the eikonalized cross section.

On the contrary, other models like the Heavy-Ion Jet Interaction Generator (HIJING) [43], Eskola *et al.* [44], and Geiger and Müller [45] are mainly focused to the hard part. They compute the number of minijets or partons with transverse momentum larger than a given $p_{\perp 0} \geq 1 \div 2$ GeV/c. These hard partons are taken [46] as the starting point of an evolution and expansion previous to hadronization (for discussions on this point see for example [47, 48]). A soft part, extracted from the SPS data, is added with an energy dependence taken from some model.

[4] ALICE (A Large Ion Collider Experiment) is the approved detector at the LHC fully dedicated to Heavy Ion Physics.

[5] Un updated set of predictions for RHIC can be found in [26].

A third kind of models are the statistical and thermodynamical ones [4, 5]. In these models the main predictions refer to ratios between different kind of particles and not to absolute values of each kind. Usually to get absolute rapidity densities the volume at freeze-out has to be specified. The volumes used are $\sim$ 3600 and $\sim$ 14400 fm^3, giving charged particle densities at midrapidity of 1200 and 8000 at RHIC and LHC energies respectively[6] .

The plan of this review will be the following: After this Introduction, in the next Section the DPM and DPMJET Monte Carlo code will be discussed in some detail, introducing several concepts which will also be used in the other models. In Sections 3, 4, 5 and 6 the SFM, RQMD, HIJING and Perturbative QCD (PQCD) and Hydrodynamical models respectively, together with their predictions for charged particle densities at midrapidity, will be briefly reviewed. Other models will be discussed in Section 7. Afterwards, in Section 8 we will argue on percolation in heavy ion collisions, and in Section 9 possible implications for Cosmic Ray Physics will be commented. In the last Section the different results will be compared and some discussions presented.

2 The Dual Parton Model and the DPMJET Monte Carlo code

The DPM [27] is a dynamical model for low $p_\perp$ hadronic and nuclear interactions, based on the large N expansion of QCD with N_c/N_f fixed [49]. The dominant lowest order configuration in p-p scattering at high energy consists in the production of two strings between valence constituents, of type $(qq)_v - q_v$, see Fig. 2.

There are also more complicated terms, corresponding to higher order diagrams in the large N expansion, involving 4, 6,... strings. These extra strings are of the type $q_s - \overline{q}_s$, with sea quarks and antiquarks at their ends (Fig. 3). These configurations correspond to multiple inelastic scattering in the S-matrix approach, the number of strings being equal to twice the number of inelastic collisions. The contribution of each configuration to the cross section is determined using the generalized eikonal approach (see below) or the perturbative Reggeon calculus [50] in hadron-hadron collisions and the Glauber-Gribov model [51, 52] in collisions involving nuclei.

For A-A collisions, the rapidity distribution of secondaries is given by [28, 29]

$$\frac{dN^{\rm AA}}{dy} = \overline{n}_{\rm A} \left[N^{(qq)_v^{{\rm A}p} - q_v^{{\rm A}t}}(y) + N^{q_v^{{\rm A}p} - (qq)_v^{{\rm A}t}}(y) \right] + 2\ (\overline{n} - \overline{n}_{\rm A})\ N^{q_s - \overline{q}_s}(y), \qquad (1)$$

[6]The value of 8000 charged particles per unit rapidity at $y = 0$ was the preferred value for many models before 1995. Indeed only the SFM gave values close to 2500. Now, by different although probably related reasons, several models have lowered their predictions to values close to the SFM one.

where $N(y)$ are the rapidity distributions of produced particles in the individual strings stretched between the projectile (p) and target (t) nuclei, $\overline{n}_{\rm A}$ is the average number of wounded nucleons of A and $\overline{n}$ is the average number of nucleon-nucleon collisions. Both $\overline{n}_{\rm A}$ and $\overline{n}$ are computed [53] in the Glauber model. For instance, for minimum bias collisions

$$\overline{n} = \frac{{\rm A}^2\sigma_{\rm NN}}{\sigma_{\rm AA}} \simeq \frac{{\rm A}^2\sigma_{\rm NN}}{\pi(2R_{\rm A})^2} \approx \frac{{\rm A}^{4/3}}{4} \ , \tag{2}$$

with $\sigma_{\rm NN}$ and $\sigma_{\rm AA}$ the nucleon-nucleon and nucleus-nucleus cross sections respectively; for central collisions,

$$\sigma_{\rm AA} \simeq \pi R_{\rm A}^2 \ , \quad \overline{n} \approx {\rm A}^{4/3}. \tag{3}$$

If all strings would have the same plateau height (i.e. the same value of $N(0)$), $dN^{\rm AA}/dy|_{y=0}$ would increase like ${\rm A}^{4/3}$. However at present energies the plateau height of the $q_s - \overline{q}_s$ strings is much smaller than that of the $(qq)_v - q_v$ ones, and the first term in (1) dominates. One obtain in this way the result of the Wounded Nucleon Model (WNM) [54]. At SPS energies only for central collisions some departure of the law [29]

$$\frac{dN^{\rm AA}}{dy} \propto \overline{n}_{\rm A} \tag{4}$$

is expected, and indeed has been seen in the experimental data [55, 56].

At higher energies the contribution of the sea strings becomes increasingly important, not only because their plateau height gets higher but also due to the need to introduce multistring configuration in each nucleon-nucleon collision. If the average number of strings in each nucleon-nucleon collision is $2\overline{k}$ (this number can be computed in the generalized eikonal model), the total number of strings is $2\overline{k}\overline{n}$ and (1) is changed into

$$\begin{aligned} \frac{dN^{\rm AA}}{dy} &= \overline{n}_{\rm A}\left[N^{(qq)_v^{{\rm A}p}-q_v^{{\rm A}t}}(y) + N^{q_v^{{\rm A}p}-(qq)_v^{{\rm A}t}}(y) + (2\overline{k}-2)N^{q_s-\overline{q}_s}(y)\right] \\ &+ 2\ \overline{k}\ (\overline{n}-\overline{n}_{\rm A})\ N^{q_s-\overline{q}_s}(y). \end{aligned} \tag{5}$$

The hadronic spectra of the individual strings $N(y)$ is obtained from a convolution of momentum distribution functions and fragmentation functions [27]. Both functions can be determined to a large extent from known Regge trajectories.

For RHIC and LHC energies $\overline{k} \sim 2$ and 3 respectively. Using these values in (5) it is obtained [57]:

$$\begin{aligned} \left.\frac{dN^{\rm SS}}{dy}\right|_{y=0} &= 170, \qquad \left.\frac{dN^{\rm PbPb}}{dy}\right|_{y=0} = 1890 \quad \text{at } \sqrt{s} = 200 \text{ GeV per nucleon}, \\ \left.\frac{dN^{\rm SS}}{dy}\right|_{y=0} &= 500, \qquad \left.\frac{dN^{\rm PbPb}}{dy}\right|_{y=0} = 7900 \quad \text{at } \sqrt{s} = 7 \text{ TeV per nucleon}, \end{aligned} \tag{6}$$

for charged particles in central ($\overline{n}_{\rm A} > 28$ in S-S and 200 in Pb-Pb, corresponding to $b \simeq 0$) A-A collisions (in [58] a value of 8500 for Pb-Pb, $b < 3$ fm, at $\sqrt{s} = 6$ TeV per nucleon is given).

In these results no semihard collisions were taken into account. The inclusion of this kind of collisions cannot modify significantly the numbers in (6) since the total number of strings is constrained by unitarity. The fact that some of the $q_s - \overline{q}_s$ strings can be the result of a semihard gluon-gluon interaction, will affect the $p_\perp$ distribution of the produced particles. However, average multiplicities are practically unchanged if one neglects changes from energy-momentum conservation due to the larger $p_\perp$ in the semihard contribution.

Other effect not taken into account in these first estimations done in 1991 [57] is shadowing corrections, which can be of importance at RHIC and LHC energies. The physical origin of shadowing corrections[7] can be traced back to the difference between the space-time picture of the interaction in the Glauber model [51] and in Glauber-Gribov field theory [52]. In Glauber we have successive collisions of the incident hadron to explain multiple scattering in hadron-nucleus interactions, while in Gribov theory simultaneous collisions of different projectile constituents with nucleons in the target nuclei are considered. Nevertheless, the h-A scattering amplitude can be written as a sum of multiple scattering diagrams with elastic intermediate states, which have the same expressions in both cases. In addition to these diagrams there are other ones which contain, as intermediate states, all possible diffractive excitations of the projectile hadron, whose influence at SPS energies is small. The size of the high mass excitations of the initial hadron is controlled by the triple Pomeron coupling. The value of this coupling, determined from soft diffraction experimental data, allows to describe hard diffraction measured at the Hadron-Electron Ring Accelerator (HERA) at DESY and also the size of the shadowing effects in the nuclear structure functions at small x [59]. These considerations imply a reduction of particle densities at midrapidity of a factor 2 at RHIC and 3 at the LHC [58].

This shadowing can be alternatively seen as a way of introducing the interaction among strings, see next Section. In (1) and (5) it is assumed that strings fragment independently one from each other. As the number of strings grows with the energy of the collision, with the size of the projectile or the target and with the degree of centrality of the collision, interaction of strings is expected at very high energies in central heavy ion collisions. This approach is equivalent to take into account the triple Pomeron coupling, whose effects on dN/dy are very small at SPS energies and become large at RHIC and LHC.

In order to include the hard part in the DPM, the eikonal depending on impact parameter

[7] For a discussion on the relation between unitarity, parton saturation and shadowing see for example [48].

b and energy is divided in a sum of soft plus hard pieces [60, 61],

$$\chi(b^2,s) = \chi_s(b^2,s) + \chi_h(b^2,s), \tag{7}$$

normalized to the corresponding elementary cross sections,

$$\int d^2b\ 2\chi_i(b^2,s) = \sigma_i^0\ , \quad i = s,h; \tag{8}$$

in terms of the eikonal, the inelastic cross section for the collision is

$$\sigma_{in} = \int d^2b\ \left[1 - e^{-2\chi(b^2,s)}\right]. \tag{9}$$

The soft eikonal is parametrized as

$$\chi_s(b^2,s) = \frac{\sigma_s^0}{8\pi\left[c + \alpha' \log\left(s/s_0\right)\right]}\ \exp\left(-\frac{b^2}{4\left[c + \alpha' \log\left(s/s_0\right)\right]}\right) \tag{10}$$

and the hard one as

$$\chi_h(b^2,s) = \frac{\sigma_h^0}{8\pi d} \exp\left(-\frac{b^2}{4d}\right). \tag{11}$$

The soft input is a soft Pomeron with a linear trajectory, $\alpha_s(t) = 1 + \Delta_s + \alpha' t$,

$$\sigma_s^0 = g^2 s_s^{\Delta}, \tag{12}$$

and the hard cross section σ_h^0 is calculated from PQCD using a lower $p_\perp$ cut-off and conventional structure functions. Unitarity of the cross section is explicit in (9), which can be expanded as

$$\sigma_{in} = \int d^2b \sum_{l_c+m_c\geq 1} \sigma(l_c, m_c, b^2, s), \tag{13}$$

the sum running over l_c soft elementary collisions and m_c hard ones.

DPMJET is a Monte Carlo code for sampling hadron-hadron, hadron-nucleus, nucleus-nucleus, lepton-hadron and lepton-nucleus collisions at accelerator and cosmic ray energies [30]. It uses the DPM for hadronic and nuclear interactions, the hard part being simulated using PYTHIA [62] and, in its latest version DPMJET-II.5 [31], one of the most recent sets of parton distribution functions, GRV-LO-98 [63]. The code includes intranuclear cascade processes of the created secondaries with formation time considerations, and also nuclear evaporation and fragmentation of the residual nucleus.

In the first versions of the code, in addition to diagrams where the valence diquarks at the end of one string fragment into hadrons preserving the diquark, diquark breaking was allowed. This is the so-called popcorn mechanism, see Fig. 4. However the mechanism is not enough to explain the large baryon stopping observed in A-B collisions. For this reason in the DPM new diagrams [19, 20, 64, 65] for diquark breaking, like the one in Fig. 5, have

been proposed and discussed. In both Figs. 4 and 5 the dashed line is the string junction: at large N_c a baryon can be pictured [66] as made out of three valence quarks together with three strings which join in the string junction[8] . These diagrams, included in DPMJET-II.5, shift the baryon spectrum to the central rapidity region and also produce an enhancement of strange baryons and antibaryons.

In the code the presence of diquarks and antidiquarks at sea string ends is also included. This increases baryon and antibaryon rapidity densities and, due to energy-momentum conservation, reduces that of pions.

The results of DPMJET-II.5 for charged particles in central Pb-Pb collisions at RHIC (3 % more central events) and LHC (4 % more central events) are [31]

$$\left.\frac{dN}{dy}\right|_{y=0}^{\rm RHIC} = 1280, \quad \left.\frac{dN}{dy}\right|_{y=0}^{\rm LHC} = 2800. \tag{14}$$

These values agree with the ones computed in the DPM [58], see above. The previous version of the code [30] gives a higher value at LHC, $dN_{ch}/d\eta|_{\eta=0} = 3700$ [22] (although for $\sqrt{s} = 6$ TeV per nucleon and $b \leq 3$ fm). This reduction is due to the inclusion of new diagrams and to the energy-momentum conservation consequences of the inclusion of $(qq)_s - (\overline{qq})_s$ strings. Notice than the value obtained in the code is much smaller than that obtained in the DPM using (5). This fact is essentially due to energy-momentum conservation, which prevents some of the ($\overline{n}$,$\overline{n}_{\rm A}$,$\overline{k}$) configurations to take place.

3 The String Fusion Model

The SFM [23, 34, 35] is based on QGSM, a model which is quite similar to DPM with only minor differences. The main ingredient added in the SFM is the fusion of strings [68, 69]. The basic idea is that strings fuse as soon as their transverse position come within a certain interaction area, of the order of the string proper transverse dimension as dictated by its mean $p_\perp$. In a Monte Carlo approach, such a picture can be realized by assuming that strings fuse as soon as partons which act as their sources, have their transverse positions close enough. In this language the fusion probability is determined by the parton transverse dimension, that is, by the parton-parton cross section. Energy conservation can be taken into account by distributing the available energy among these active partons, as it has always been done in string models [27, 32]. Then the emerging strings occupy different intervals in rapidity space, determined by the energy-momentum of their sources. The fusion of strings may only take place when their rapidity intervals overlap. In particular, for two pairs of

[8] Using some supergravity solution and the recently conjectured duality between gauge and string theory the large N_c baryon wave function has been constructed from N_c strings connected via a junction [67].

partons from the projectile and target with rapidities y_1, y_2 and y_1', y_2' respectively, the two corresponding strings fuse in the interval $[\max\{y_1', y_2'\}, \min\{y_1, y_2\}]$. If this interval becomes small the resulting object will have will have its total energy of the order of a typical hadron mass and, as with ordinary strings, is no more a string but rather an observed hadron. The exact value of the minimal string energy and thus of its minimal rapidity length is taken the same as for ordinary strings.

The color and flavor properties of the formed strings follow from the properties of their ancestor strings. The fusion of several quark-antiquark $q-\overline{q}$ strings produces a $Q-\overline{Q}$ complex with color Q (quadratic Casimir operator of the representation Q^2), which is determined by the SU(3) color composition laws. For example, the fusion of two $q-\overline{q}$ triplet strings produces a $[\overline{3}]$ string (that is, a diquark-antiquark string) with probability 1/3 and a [6] string with probability 2/3 ($[3] \otimes [3] = [6] \oplus [\overline{3}]$). On the other hand, if two triplet strings with opposite color flux directions fuse (a quark [3] state fuses with a $[\overline{3}]$ antiquark state), either colorless states at the end of the new string or a [8] string are formed with probabilities 1/9 and 8/9 respectively ($[3] \otimes [\overline{3}] = [1] \oplus [8]$). The flavor of the fused string ends is evidently composed of the flavor of the partons sitting there. As a result of string fusion, we thus obtain strings with arbitrarily large color and differently flavored ends, in accordance with the probability to create the color Q from several (anti)quarks. Crude characteristics of hadron interactions depend only on the fact that the total number of strings of whatever color in a given transverse area becomes limited because of their fusion. In other words, string density cannot grow infinitely but is bounded from above [68]. More detailed properties of hadron spectra require knowledge of a particular manner in which the new fused strings decay into hadrons.

In all color string models, it is assumed that the homogeneous color field corresponding to the strings creates pairs of colored partons, which neutralize this field and provide for its subsequent decay. The basic formula which describes the probability of such a process is taken in the spirit of the famous Schwinger expression for the probability to create an electron-positron pair in a constant electromagnetic field [70, 71, 72]. With a constant color field which originates from two opposite color charges $\vec{Q}$ and $-\vec{Q}$ (8-vectors in SU(3)), the probability rate to create a pair of partons with color charges $\vec{C}$ and $-\vec{C}$, flavor f and mass M_f for unit string length is assumed to be given by

$$\frac{d\omega(\vec{Q}, \vec{C})}{d^2 p_\perp} \propto A_t \ (kQC)^2 \ \exp\left(-\frac{M_\perp^2}{kQC}\right) . \tag{15}$$

The parameter A_t has the meaning of the string transverse area and $M_\perp$ is the transverse mass. k is proportional to the string tension κ,

$$\kappa = \frac{\pi k Q^2}{2} . \tag{16}$$

In [72, 73] the strings of high color, denoted as color ropes, break as a result of successive production of $q\overline{q}$ pairs, which gradually neutralize the color flux of the string until it breaks. In SFM, however, the process considered is that of creation of a pair of parton complexes with color $\vec{Q}$ equal to that of the ends of the string. This is the main contribution to the breaking of the string for low values of Q [23]. As, in the Monte Carlo code, fusion of strings is taken into account in an effective way and only fusion of two strings is allowed, the mechanism of string breaking for high color strings is the one just mentioned. It is also assumed that [3], $[\overline{3}]$, [6] and [8] strings have the same transverse area[9] . The string tension is proportional to Q^2,

$$Q^2_{[3]} = 4/3 = Q^2_{[\overline{3}]}, \quad Q^2_{[8]} = 3, \quad Q^2_{[6]} = 10/3. \tag{17}$$

So, approximately $\kappa_{[8]} \sim \kappa_{[6]} \sim 2.5\ \kappa_{[3]} = 2.5\ \kappa_{[\overline{3}]}$.

As can be inferred from what has been presented above, fusion of strings leads to an enhancement of baryon and antibaryon production, due to the possibility of having (qq) and $(\overline{qq})$ at the end of the fused strings. In DPM a similar mechanism is introduced considering the possibility of diquarks in the sea, as mentioned in the previous Section. In addition to this mechanism there is another source of baryon enhancement, due to the larger tension of fused strings (17) which, through (16) and (15), implies a more efficient production of heavy quarks and diquarks, and of higher $p_\perp$. Therefore, it is also expected heavy flavor enhancement and some increase of transverse momentum.

Another important consequences of string fusion is the possibility of producing particles in collisions involving nuclei, outside the nucleon-nucleon kinematical region, the so-called cumulative effect (part of these effect is usually addressed to the Fermi motion of nucleons inside nuclei). In fact the resulting fused string has an energy-momentum corresponding to the sum of the energy-momenta of its ancestor strings, which can be larger than the energy-momentum available in an isolated nucleon-nucleon collision [77].

In the SFM code, the nuclear parton wave function is taken as a convolution of the parton distribution in a nucleon with the nucleon distribution in a nucleus. In this way, hadrons and nuclei are treated in a similar way, different from what DPMJET does. Also, in a previous version of SFM [23] most of the computations where done at SPS energies and no hard part was considered. This part is now introduced in the code in a standard way [35] and modifies the central rapidity region at energies higher than those of SPS.

The probability of fusion of two strings is controlled by the parton-parton cross section,

$$\sigma_p = 2\pi r^2. \tag{18}$$

[9]This assumption is a very strong one; other possibilities will be discussed in Section 8 in relation to percolation of strings [16, 74, 75, 76].

Its numerical value is fixed to $\sigma_p \simeq 8$ mb, in order to reproduce the $\overline{\Lambda}$ enhancement seen in central S-S and S-Ag collisions at SPS energies [78]. This value, which means $r \sim 0.36$ fm, has been obtained implementing in the code fusion of only two strings and therefore has to be considered as an effective one. The actual transverse size of a string should be less, a more realistic one being $r \simeq 0.2 \div 0.25$ fm [16], a value which agrees with other considerations [74, 79, 80].

For the purpose of this review, the most important consequence of fusion of strings is that it suppresses total multiplicities, reducing the number of pions in the central rapidity region, although the rapidity distribution becomes larger at the extreme of the fragmentation regions. In the predictions done with the previous version of the model [23], no hard part was included and the charged particle densities at midrapidity for central ($b = 0$) Au-Au collisions were

$$\begin{aligned} \left.\frac{dN}{dy}\right|_{y=0} &= 1000 \quad \text{at } \sqrt{s} = 200 \text{ GeV per nucleon}, \\ \left.\frac{dN}{dy}\right|_{y=0} &= 1900 \quad \text{at } \sqrt{s} = 6.3 \text{ TeV per nucleon}. \end{aligned} \tag{19}$$

The corresponding values without considering fusion of strings were 1850 and 4000 respectively. A strong suppression of the central density is produced (note the agreement with the values from DPMJET). Including the hard part [35], the values for collisions of charged particle densities corresponding to the 5% more central events[10] are

$$\begin{aligned} \left.\frac{dN^{\mathrm{AuAu}}}{dy}\right|_{y=0} &= 910 \quad \text{at } \sqrt{s} = 200 \text{ GeV per nucleon}, \\ \left.\frac{dN^{\mathrm{PbPb}}}{dy}\right|_{y=0} &= 3140 \quad \text{at } \sqrt{s} = 5.5 \text{ TeV per nucleon}, \end{aligned} \tag{20}$$

and now the suppression due to string fusion is smaller (the corresponding values without fusion are 1300 and 3690 respectively). The reason for this is that the strings coming from hard scatterings do not fuse in the code. At LHC a large proportion of strings are hard ones and therefore the relative size of suppression is smaller. The hard strings have a size $\sim 1/p_\perp$ and indeed should interact and fuse, although with smaller probability than the soft ones. Effects of overlapping of strings will be further discussed in Section 8.

4 The Relativistic Quantum Molecular Dynamics Model

RQMD [36, 37, 38] is a semiclassical microscopic approach which combines classical propagation with stochastic interactions. Strings and resonances can be excited in elementary

[10] In the model, this translates into $b \leq 3.2$ fm for Au-Au at RHIC and $b \leq 3.3$ fm for Pb-Pb at LHC.

collisions, their fragmentation and decay leading to the production of particles. The nature of the active degrees of freedom in RQMD depends on the relevant length and time scales of the processes considered. In low energy collisions (around 1 GeV per nucleon in the center of mass) RQMD reduces to solving transport equations for a system of nucleons, other hadrons and eventually resonances interacting in binary collisions and via mean fields. At large beam energies ($>$ 10 GeV per nucleon in the center of mass) the description of a projectile hadron interacting in a medium (a cold nucleus) as a sequence of separated hadron or resonance collisions breaks down. A multiple collision series is formulated on the partonic level, following the Glauber-Gribov picture. In RQMD these multiple collisions correspond to strings formed between partons of the projectile and target, including sea quarks and antiquarks. The string excitation law $dP \propto dx^+/x^+$ is the same used in FRITIOF [33]. The decay of elementary color strings is done using JETSET [81]. Rescattering is included: four classes of binary interactions, BB, BM, MM and $\overline{\mathrm{B}}$B (B denoting baryon, M denoting meson) are considered.

One of the main ingredients of RQMD is the inclusion of interaction of strings by means of formation of color ropes, see previous Section, when there are overlapping strings. These ropes are chromoelectric flux tubes whose sources are charge states in representations of color SU(3) with dimension higher than the triplet one. They are equivalent to the fused strings of SFM. As already mention, as a simplification in SFM only fusion of two strings is considered, as an effective way to take into account string interaction. In RQMD all possibilities are considered. The breaking of these higher color strings proceeds through successive production of $q\overline{q}$ pairs [72, 73] due to the Schwinger mechanism.

As in the case of SFM, introduction of color ropes in RQMD leads to heavy flavor and baryon and antibaryon enhancement. In version RQMD 2.3 the model reproduces the SPS rapidity distributions of h^-, K^0, Λ, $\overline{\Lambda}$, Ξ^- and $\overline{\Xi}^+$. It slightly underestimates the yields of Ω^- and $\overline{\Omega}^+$ (by less than a factor 2). Also it is able to reproduce the $m_\perp$ spectrum of all these particles. Let us mention that independent string models are not able to reproduce these slopes.

The formation of color ropes leads to a strong suppression of central rapidity distributions. The prediction of RQMD for central ($b = 3$ fm) Pb-Pb collisions at RHIC is $dN/dy|_{y=0} \simeq 700$ [26, 82]. This number is lower than the value of SFM, 910. The reason for that probably has to do with the strong fusion probability used in RQMD. The effect of this strong string interaction in some observables (like antibaryon enhancement) is compensated by other processes (a large $\overline{\mathrm{B}}$B annihilation).

5 The Heavy-Ion Jet Interaction Generator (HIJING)

In HIJING [43] the soft contribution is modeled by diquark-quark strings with gluon kinks induced by soft gluon radiation, in a way very similar to the FRITIOF model [33]. Since this model treats explicitly minijet physics through PQCD, the transverse momentum in string kinks due to soft processes is limited from above by a minijet scale $p_{\perp 0} = 2$ GeV/c. Gluon radiation is extended to the hard part of high $p_\perp$, which, together with the use of momentum distribution functions for partons similar to those of DPM, constitutes a difference with FRITIOF. Strings decay independently by means of the JETSET [81] routines. In addition to the low $p_\perp < p_{\perp 0}$ gluon kinks, HIJING includes an extra low $p_\perp$ transfer between the constituent quarks and diquarks at the string ends. This extra $p_\perp$ is chosen to ensure an smooth extrapolation in the $p_\perp$ distributions from the soft to the hard regime.

Multiple minijet production with initial and final state radiation is included along the lines of the PYTHIA model [62]. First, the cross section for hard parton scattering σ_{jet} is computed in PQCD at leading order (LO), using a K-factor $\simeq 2$ to simulate higher order corrections. The eikonal formalism, see Section 2, is employed to calculate the number of minijets per inelastic nucleon-nucleon collision. For A-A collisions at impact parameter b the total number of jets is given by

$$N_{jet}^{\rm AA}(b) = \frac{{\rm A}^2\ T_{\rm AA}(b)}{\sigma_{\rm AA}(b)}\ \sigma_{jet}\ , \tag{21}$$

with

$$T_{\rm AA}(b) = \int d^2b'\ T_{\rm A}(b-b')T_{\rm A}(b'), \tag{22}$$

$T_{\rm A}(b)$ being the nuclear profile function normalized to 1 and $\sigma_{\rm AA}(b) \simeq \int d^2b\ \{1-\exp\left[-\sigma_{\rm NN}A^2T_{\rm A}(b)\right]\}$ the A-A cross section [29, 53] for impact parameter b. For central collisions $b = 0$, $\sigma_{\rm AA}(b = 0) \simeq 1$ and

$$N_{jet}^{\rm AA}(b) \approx \frac{{\rm A}^2}{\pi R_{\rm A}^2}\ \sigma_{jet} \propto {\rm A}^{4/3}\ . \tag{23}$$

Therefore, at high energies and for central nucleus-nucleus collisions there will be many minijets.

In the model, jet quenching [83] is included to enable the study of the dependence of moderate and high $p_\perp$ observables, on an assumed energy loss per unit length dE/dx of high energy partons traversing the dense matter produced in the collision. The effect of including jet quenching is a moderate enhancement of particle production in the central rapidity region and to diminish the yield in the fragmentation regions. Furthermore, in the last version of the model the mechanism of string junction migration [19] explained in Section 2 is included, in order to shift baryons from fragmentation to central rapidity regions.

The results for charged densities at midrapidity in central ($b < 3$ fm) Au-Au collisions at $\sqrt{s} = 200$ GeV per nucleon are shown in Fig. 6. The different curves refer to different versions of the model with and without quenching and shadowing of the nucleon structure functions in the nucleus [43, 84]. For LHC, HIJING predictions [43] lie in the range $5000 \div 7500$ depending on structure functions used and quenching included or not.

6 Perturbative Quantum Chromodynamics and Hydrodynamical models

It has been argued [46] that the initial state (the initial distribution of partons) in a high energy heavy ion collision could be computed using PQCD. Several groups [44, 45] have developed models along this line. Concretely, Eskola *et al.* have computed [44] charged densities and transverse energies al midrapidities, using PQCD at some given scale which is taken to be equal to a saturation scale, the scale at which parton distributions stop their increasing at small x.

In ultrarelativistic heavy ion collisions the number of produced gluons and quarks with $p_\perp$ greater than some cut-off p_0, $N_{\rm AA}\left(b, p_0, \sqrt{s}\right)$, increases when p_0 decreases, when the size of the nuclei increases or b decreases, see (21) and (23), and when $\sqrt{s}$ increases due to the small x enhancement of parton distribution functions. Shadowing of nucleon structure functions in nuclei will decrease $N_{\rm AA}\left(b, p_0, \sqrt{s}\right)$, but next-to-leading order (NLO) corrections will increase it. At sufficient large cut-off $p_0 \gg \Lambda_{\rm QCD}$ the system of produced gluons is dilute and usual perturbation theory is applicable. However, at some transverse momentum $p_0 = p_{sat}$ the gluon and quark phase space density saturate and no further increase is expected. In this case one may conjecture that evaluation of the number of charged particles N_{ch} and transverse energy E_T using QCD formulae at this saturation scale p_{sat} gives a good estimate of the total N_{ch} and E_T (partons with $p_\perp \gg p_{sat}$ are rare, partons with $p_\perp \ll p_{sat}$ saturate and contribute little to the total E_T).

In [44], first $N_{\rm AA}\left(b = 0, p_0, \sqrt{s}\right)$ for $|y| < 0.5$ is computed using standard PQCD expressions at LO. Nuclear effects on parton distribution functions are implemented using the EKS98 parameterization [84] of nuclear corrections. To simulate NLO contributions, a K-factor K = 2 is used. The scale in the PQCD calculation is fixed from considering that at saturation $N_{\rm AA}(b = 0, p_{sat}, \sqrt{s})$ partons, each one with transverse area π/p_{sat}^2, fill the whole transverse area $\pi R_{\rm A}^2$,

$$N_{\rm AA}\left(b = 0, p_{sat}, \sqrt{s}\right) = p_{sat}^2 R_{\rm A}^2 \ . \tag{24}$$

In Fig. 7 $N_{\rm AA}\left(b = 0, p_0, \sqrt{s}\right)$ is plotted for A = 208 as a function of p_0 at SPS, RHIC and LHC energies. The dashed curve is $p_0^2 R_{\rm A}^2$. The intersection points give us p_{sat} at the corresponding

energies. Of course, all this is only valid as long as $p_0 \gg \Lambda_{\rm QCD}$ for perturbation theory to be justifiedly used, which is doubtful at SPS and RHIC (see the Figure; the saturation momentum are ~ 0.5, ~ 1.4 and ~ 2.3 GeV/c at SPS, RHIC and LHC energies respectively).

The values of $N_i = N_{\rm AA}\,(b=0, p_{sat}, \sqrt{s})$ and p_{sat} can be well fitted by the expressions

$$N_i = 1.383\ {\rm A}^{0.922}\ (\sqrt{s})^{0.383}\ , \tag{25}$$

$$p_{sat} = 0.208\ {\rm A}^{0.128}\ (\sqrt{s})^{0.191}\ \ {\rm GeV/c}. \tag{26}$$

The initial state computed in this way very nearly fulfills the kinetic thermalization condition for bosons, $\epsilon/n = 2.7\ T$ (the number of gluons is much larger than that of quarks), and there also is some justification to consider that further hydrodynamical expansion is locally thermal, i.e. entropy conserving. Thus initially the entropy $S_i = 3.6\ N_i$ (ideal system of bosons). For the final hadronic gas $S_i = S_f \simeq 4\ N_f$ so that $N_f = 0.9\ N_i$, i.e. the number of hadrons in the final state is, up to 10 % corrections, equal to the number of initially produced gluons at the scale p_{sat}. The multiplicity prediction [44, 26]

$$N_{ch} = \frac{2}{3}\ 0.9\ N_i \tag{27}$$

is directly obtained from (25) and plotted as a dashed line in Fig. 8. The values at RHIC and LHC for central ($b = 0$) Pb-Pb collisions are 900 and 3100, not very different from those obtained by DPM, DPMJET and SFM on very different grounds[11] .

7 Other models

In this Section we would like to comments on some other models. The fact that the rest of the models are joined together, do not mean at all that they are less important or successful than the mentioned ones. It is simply the shortage of space which prevents us from a longer study.

The VENUS model [24] is an extension of DPM. The main difference is the inclusion of diagrams in which there is two color exchanges, the first one providing two $(qq)_v - q_v$ strings, one of the being intermediate, because a second color exchange breaks the diquark, giving a different $(qq)_v - q_v$ string and a double string which consists in a forward moving quark linked to two backward moving quarks, see Fig. 9. These diagrams become increasingly important with a growing number of inelastic collisions, as in h-A or A-B, although of course they are also present in N-N collisions. They enhance stopping power, shifting the baryon spectrum towards midrapidities.

[11] Theoretical models based on a semiclassical treatment of gluon radiation [85] by partons in the colliding nuclei give values compatible with these ones, see [86].

VENUS gives large values for central rapidity densities. At $\sqrt{s} = 6$ TeV per nucleon for central ($b \leq 3$ fm) Pb-Pb collisions its result is $dN_{ch}/d\eta|_{\eta=0} = 8400$ [22]. The model has lately been extended to deal with γ^*-γ^*, γ^*-h, ν-h, h-h, h-A and A-B collisions in the same unified approach [41]. An unique Pomeron describes both soft and hard interactions by means of the evolution of structure functions from some properly chosen initial conditions. The new model [41], denoted by NEXUS, has not given values for LHC yet. Preliminary predictions for central ($b < 2$ fm) Au-Au collisions at RHIC are $dN_{ch}/dy|_{y=0} \simeq 1100$ [26]. In this model particles and resonances produced in string fragmentation are allowed to rescatter and, if more than two of them are close enough, joined into a quark cluster which is decayed isotropically [87].

The LUCIAE event generator [42] (Lund University and China Institute of Atomic Energy) is a version of the FRITIOF model [33] where collective interactions among strings and rescattering of the produced particles are included. The collective interactions are incorporated following [88]. LUCIAE has studied several observables at SPS comparing to experimental data, but, to our knowledge, has not worked out predictions for rapidity densities at RHIC and LHC. In any case, the inclusion of collective string effects produces very fast particles [73] at the extreme of the phase space, similar to the cumulative effect which occurs in the SFM. Also, simply by energy-momentum conservation, a suppression of particles in the central rapidity region should happen.

The Ultrarelativistic Quantum Molecular Dynamics (UrQMD) [39, 40] is a microscopic hadronic approach based on the covariant propagation of mesonic and baryonic degrees of freedom. It allows for formation of strings and resonances, and rescattering among them and of the produced particles. In this aspect it is quite similar to RQMD. In the low energy region, i.e. $\sqrt{s} \leq 2$ GeV per nucleon, the inelastic cross sections are dominated by s-channel formation of resonances, which decay into particles isotropically in their local rest frame according to their lifetimes. A large variety of baryonic and mesonic states have been incorporated in the model. All corresponding antiparticles are included and treated on the same footing. At higher energies strings are considered. Much attention is paid in the model to the intermediate energy region between AGS, the Alternating Gradient Synchrotron at BNL ($\sqrt{s} \sim 5$ GeV per nucleon), and SPS, in order to achieve a smooth transition between the low and high energy regimes. The prediction of the model [40, 26] for central ($b \leq 3$ fm) Au-Au collisions at RHIC is shown in Fig. 10. The central density of charged pions is ~ 750, being for all charged particles ~ 1100.

Another approach using also UrQMD is the model denoted by VNI+UrQMD, where a combined microscopic partonic/hadronic transport scenario is introduced [89]. The initial high density partonic phase of the heavy ion reaction is calculated in the framework of the

parton cascade model VNI [90], using cross section obtained from PQCD at LO (see [91] for a discussion of the uncertainties introduced by NLO corrections and K-factors in VNI and other parton cascade models). The partonic state is then hadronized via a configuration space coalescence and cluster hadronization model, and used as initial condition for a hadronic transport calculation using UrQMD. In Fig. 11 the time evolution of parton and on-shell hadron rapidity densities for central ($b \leq 1$ fm) at RHIC can be seen [89, 26]. From this curve, the charged particle rapidity density is ~ 1000. When, instead of calculating the initial phase using a parton cascade approach, QGP formation is assumed, this plasma is evolved hydrodynamically until hadronization, and then UrQMD is used for hadronic transport (the model considers a first order phase transition and is denoted as Hydro+UrQMD [92]), a smaller charged particle central rapidity density is obtained for central ($b = 0$) Au-Au collisions at RHIC, ~ 750.

Using also VNI there is the model denoted by VNI+HSD [93], where HSD stands for Hadron String Dynamics model [94]. This model involves quarks, diquarks, antiquarks, antidiquarks, strings and hadrons as degrees of freedom. The parton cascade model VNI is extended by the hadronic rescattering as described by HSD. Its results for central ($b \leq 2$ fm) Au-Au collisions at RHIC are shown in Fig. 12, where VNI and HSD predictions are the four plots at the top and VNI+HSD are the two plots at the bottom. It is worth noting that VNI+HSD gives almost the same results as HSD, which already includes final state interactions. This fact, also observed in DPM and SFM (see Section 2) is based on unitarity, which controls the number of inelastic collisions independently of their soft or hard origin. The total number of charged particles at midrapidity is ~ 1150.

Another RHIC prediction [95, 26] comes from a modification of the HIJING model to include a parton cascade model [96] and final state interactions based on the ART model [97]. In this model (HIJING+ZPC+ART) the central rapidity density of charged particles for central ($b = 0$) collisions at RHIC is of the order 1100.

The assumption that local thermodynamical equilibrium is attained by the system of two heavy ions colliding at high energies is a basic hypothesis of macroscopic statistical and thermodynamical models [98, 99, 100, 101] (see [102] for a discussion on statistical equilibrium in heavy ion collisions). This idea comes from a long time ago [103, 104, 105]. Following [5, 101, 26] the statistical model treats the system as a grand canonical ensemble with two free parameters, a temperature T and a chemical potential μ_B. Interactions of the produced particles are taken into account considering a excluded volume correction, corresponding to repulsion setting in for all hadrons at a radius of 0.3 fm (a hard core). Hadron yield ratios resulting from this model are in reasonable agreement with SPS central Pb-Pb data. Taking these results and looking at the expected phase boundary between the QGP and the

hadron gas, the hadrochemical freeze-out points are where one expects, this being suggestive that hadron yields are frozen at the point when hadronization of the QGP is complete. This gives for RHIC a freeze-out temperature of 170 MeV, the same as found at SPS. The chemical potential is expected to be small, 10 MeV used as an upper limit. Strangeness and I_3 conservation then require values of $\mu_s = 2.5$ MeV and $\mu_{I_3} = -0.2$ MeV. In order to predict absolute yields one has to estimate the volume per unit rapidity at the time when hadronization is complete. Starting from an initial temperature of $T_i = 500$ MeV at a time $\tau = 0.2$ fm/c and using a transverse expansion with $\beta = 0.16$, this volume is 3600 fm^3 at the freeze-out temperature of 170 MeV. The number of charged pions per unit rapidity at $y = 0$ is 1260, that of charged kaons 194, that of protons 62 and that of antiprotons 56. Modifying the freeze-out temperature to 160 MeV results in a reduction of hadron yields about 10 %. For central Pb-Pb collisions at the LHC, taking again $T_f = 170$ MeV and $\mu_B = 10$ MeV and performing similar calculations, the fireball volume per unit rapidity at chemical freeze-out is 14400 fm^3, resulting in 5000 charged pions, 770 charged kaons, 250 protons and 220 antiprotons per unit rapidity. The total charged particle density is

$$\left.\frac{dN}{dy}\right|_{y=0} = 7560. \tag{28}$$

As at RHIC, small modifications of T_f and μ_B lead to small changes in this prediction. Both at RHIC and LHC the centrality of these results should correspond roughly to the centrality of the SPS experimental data which were fitted to extract the parameters used in the predictions. As different experiments consider different centrality criteria, this is not fully determined, so let us take $5 \div 10$ % as an estimate.

The quark coalescence model [26] assumes that at RHIC a QGP will be produced in the collision, which will expand and cool, hadronization proceeding via quark coalescence as described by the ALCOR model [106]. In this nonlinear coalescence model, subprocesses are not independent, competing one with each other. The coalescence equations relate the number of hadrons of a given type to the product of the numbers of different quarks from which the hadron consists. The main predictions of the model relates different particle ratios, but unfortunately the absolute values cannot be obtained in the model.

Finally, let us mention an extrapolation done by the WA98 Collaboration [56] from central pseudorapidity densities measured at SPS at different centralities. The predicted maximum charged pseudorapidity density for central Pb-Pb collisions is 1000 at RHIC and 2500 at LHC, for ~ 10 % more central events.

8 Percolation

In many models, multiparticle production at high energies is described in terms of color strings stretched between the projectile and target, see previous Sections. In principle, these strings fragment independently, the only correlation among them being energy-momentum conservation. However, with growing energy, centrality and/or size of the colliding particles, the number of strings grows and one expects that the hypothesis of independent fragmentation is no longer valid, interaction among them becoming essential. For these reasons we have seen in Section 3 and 4 different ways of taking into account such interaction. In particular, in SFM or RQMD the strings fuse or form color ropes, in such a way that the transverse size of the new string or rope is the same as that of the original strings. In this case it can be shown that there is no phase transition. However, other possibilities could be discussed. It could be the case that the new string would have a transverse size corresponding to the sum of the sizes of the original strings. In this case, a first order phase transition occurs [75].

An alternative and natural way to the formation of a (non-thermal) QGP is percolation of strings [16, 74, 107], which in any case can be used as an estimation for the failure of the independent fragmentation hypothesis. This a purely classical, geometrical mechanism. At a given energy and impact parameter b in an A-B collision, there is an available transverse area. For simplicity, let us take A=B and $b = 0$, so this area is $\pi R_{\rm A}^2$. Inside it, the strings formed in the collision can be viewed as circles of radius r_0. Some of the circles may overlap and then form clusters of strings. Above a critical density of strings, percolation occurs, so that clusters of overlapping strings are formed through the whole collision area. Percolation gives rise to the formation of a collective state, which can be identified as QGP, at a nuclear scale. The phenomenon of continuum percolation is well known and has been used to explain many different physical processes [108]. The percolation threshold η_c is related to the critical density of strings n_c by

$$\eta_c = \pi r_0^2 \, n_c \, , \tag{29}$$

$$n_c = \frac{N_c}{\pi R_{\rm A}^2} \quad \text{at} \quad b = 0, \tag{30}$$

where N_c is the number of exchanged strings and $r_0 \simeq 0.2 \div 0.25$ fm [16, 74, 79, 80], see Section 3. η_c has been computed using Monte Carlo simulation and direct connectedness expansions [108]. The results lie in the range $1.12 \div 1.18$ using step functions for the profile function of the nucleus (i.e. strings homogeneously distributed in the whole transverse area available). The use of Woods-Saxon or Gaussian nuclear densities leads to higher values of η_c [109], up to ~ 1.5. The corresponding value of n_c lies in the range $6 \div 12$ strings/fm^2. In Table 1 we show the number of strings exchanged in different central ($b = 0$) collisions

together with their densities, as obtained in the SFM [35]. It is seen that percolation could already occur for Pb-Pb at SPS. At RHIC and LHC, even collisions between much lighter nuclei could lead to the phase transition.

Table 1: Number of strings (upper numbers) and their densities (in strings/fm^2, lower numbers) for different central ($b = 0$) collisions at SPS, RHIC and LHC energies, as obtained in the SFM [35].

$\sqrt{s}$ (GeV per nucleon)	p-p	S-S	Pb-Pb
19.4	3.4	144	1365
	1.7	3.4	9.2
200	4.3	223	2029
	2.1	5.2	13.7
5500	5.8	416	3469
	2.9	9.8	23.4

Notice that string percolation occurs in two dimensions. Percolation of hadrons was proposed long ago [110] as a possible way to reach QGP. However, in this case percolation is three-dimensional and the critical density is below even normal nuclear matter density. This is in agreement with lattice studies [80] which show that the so-called energy radius of the hadron is about 0.2 fm. Therefore the color fields inside hadrons occupy only a few percent of the transverse area, $(r_0/R_h)^2 \approx (1/5)^2$. This also explains the relative weak string-string interaction (for instance the triple Pomeron coupling of Glauber-Gribov theory used in DPM and DPMJET, see Section 2).

Percolation is a second order phase transition [108]. The corresponding scaling law gives the behavior of the number of clusters of n strings, ν_n, in terms of η,

$$\langle \nu_n \rangle = n^{-\tau} \mathcal{F}\left(n^{\sigma}\left[\eta - \eta_c\right]\right), \quad |\eta - \eta_c| \ll 1, \quad n \gg 1, \tag{31}$$

where $\tau = 187/91$ and $\sigma = 36/91$. The fraction ϕ of the total surface occupied by strings is determined by

$$\phi = 1 - e^{-\eta}. \tag{32}$$

It can be seen [75] that the multiplicity μ_n due to a cluster of n overlapping strings, compared to the multiplicity of one string μ_1, is given by

$$\mu_n = n\ \mu_1\ F(\eta), \tag{33}$$

$$F(\eta) = \sqrt{\frac{1 - e^{-\eta}}{\eta}}\ . \tag{34}$$

From Table 1 and taking $r_0 = 0.25$ fm, the values of $F(\eta)$ for central ($b = 0$) Pb-Pb collisions at RHIC and LHC are 0.59 and 0.46 respectively, quite close to the values of the reduction factor of multiplicities in DPM due to triple Pomeron couplings, 1/2 and 1/3 respectively, see Section 2. A naive calculation for central rapidity densities of charged particles can be done multiplying the corresponding values obtained in the SFM [35] without fusion of strings for Pb-Pb at $b = 0$, by these reduction factors $F(\eta)$. The results for RHIC and LHC are 910 and 1980 respectively (380 at $\sqrt{s} = 19.4$ GeV with $F(\eta) = 0.68$) and clearly, from the way they were obtained, should be considered as lower bounds.

Percolation, in addition to reduce central rapidity multiplicities and enhance heavy flavor production (as string fusion does), also gives rise to other consequences in long range correlations and transverse momentum correlations [76], and J/ψ suppression [74, 109]. Also, as the energy-momentum of the clusters is the sum of the energy-momentum of the original strings, a huge cumulative effect is expected.

The critical point of percolation is the fixed point of a scale transformation (renormalization group equation) which eliminates short range correlations, surviving only long range ones. Close the that point observables should depend only on η, and not on energy or nuclear size separately.

By passing, let us notice that a similar intrinsic scale has been proposed [85] in the small x physics domain, related with saturation of structure functions or minijets, which was discussed in Section 6. This quantity is defined by

$$\Lambda^2 = \frac{N_{\rm AA}(p_{sat})}{\pi R_{\rm A}^2} \ , \tag{35}$$

with p_{sat} the transverse momentum at which saturation starts. When the number of partons $N_{\rm AA}(p_{sat})$, each one with a transverse size of the order π/p_{sat}^2, verifies $\Lambda^2\pi \simeq p_{sat}^2$, partons cover the whole nuclear area. Physics should depend only on the value of Λ^2. Furthermore, the effective action [85] which describes small x physics should become critical at some fixed point of some renormalization group, the correlation functions depending only on critical exponents determined by symmetry considerations and dimensionality. Comparing with percolation, indeed $\eta/(\pi r_0^2) = N/(\pi R_{\rm A}^2)$ is formally Λ^2, with the exchange of N soft strings by $N_{\rm AA}(p_{sat})$ partons. Let us indicate that from the arguments exposed above, overlapping partons will only cover the whole transverse area $\pi R_{\rm A}^2$ asymptotically. According to (32), the transverse area S covered by $N_{\rm AA}(p_{sat})$ partons of transverse size π/p_{sat}^2 is

$$S = \pi R_{\rm A}^2 \ \left[1 - \exp\left(-\Lambda^2\pi/r_0^2\right)\right] . \tag{36}$$

9 Cosmic Ray Physics and heavy ion accelerators

Usually it is considered that the highest cosmic ray energies, say $10^{15} \div 10^{20}$ eV, are much higher than energies reached at accelerators. With the advent of RHIC and LHC, this is not true any longer. Pb-Pb collisions at RHIC and LHC will reach total energies of $\sim 10^{15}$ and $\sim 10^{18}$ eV respectively. This means that, although no participant nuclei larger than Fe is expected, there will be collective physics to explore in Cosmic Ray Physics. In particular changes in the multiplicity originate [111] changes in the development of atmospheric showers. Unfortunately, atmospheric showers are dominated by forward particles, and it is in the fragmentation regions where models which in the central rapidity region are quite different, are more similar. Nevertheless, collective effects like color rope formation will influence the fragmentation regions (for example, the enhancement of the cumulative effect) and have observable effects in the development of the shower [77, 112]. Besides, PQCD effects may be of importance for the transverse broadening of the shower. It would be convenient to apply the different models for multiparticle production to simulations of cosmic ray atmospheric showers [113, 114].

10 Conclusions

In Table 2 predictions of the different models for charged particle densities produced in central Au-Au or Pb-Pb collisions at RHIC and LHC are presented, together with the corresponding centrality criteria. Some of the predictions of the models are not available and its place has been left empty. In order to estimate the discrepancy between different predictions induced by different definitions of centrality, by the fact that some of the results are $dN/dy|_{y=0}$ and other $dN/d\eta|_{\eta=0}$, and by using Au-Au or Pb-Pb at RHIC or slightly different energies at LHC, in Table 3 we present results obtained in the SFM [35] for different reactions. From them it can be concluded that results should be compared allowing for a $20 \div 30$ % discrepancy.

For completeness, we have included predictions from percolation and from the WNM [54]. As discussed in Section 8, the former should be considered as lower bounds. The latter have been obtained computing in SFM [35] $dN_{ch}/dy|_{y=0}$ for p-p, p-n and n-n collisions at the corresponding energies, making an isospin weighted average and multiplying by the number of wounded nucleons in a central collision, taking $\overline{n}_{\rm A} = 200$ in Pb-Pb and $\overline{n}_{\rm A} = 190$ in Au-Au (which correspond to $b \simeq 0$); the result that we get in this way for Pb-Pb at $\sqrt{s} = 17.3$ GeV per nucleon (SPS) is 370. In the following we will not discuss these two quite naive predictions.

At RHIC energies all the predictions are in the range $700 \div 1550$ and most of them in $1000 \div 1100$. The lowest value corresponds to RQMD. The reason for that, as already

Table 2: Predictions of different model for charged particle densities in central collisions. Unless otherwise stated, predictions refer to dN/dy at $y = 0$, for Au-Au at $\sqrt{s} = 200$ GeV per nucleon at RHIC and Pb-Pb at $\sqrt{s} = 5.5$ TeV per nucleon at LHC. The centrality criteria and the references from which the results have been taken are indicated in each case.

Model	RHIC	LHC
DPM	1000	2500
($\overline{n}_{\rm A} > 200$) [58]	(Pb-Pb)	($\sqrt{s} = 7$ TeV per nucleon)
DPMJET	1280	2800
[31]	(Pb-Pb, 3 %)	(4 %)
SFM	910	3140
(5 %) [35]		
RQMD	700	
[26, 82]	($b = 3$ fm)	
HIJING	$600 \div 1150$	$5000 \div 7500$
($dN/d\eta$ at $\eta = 0$, $b < 3$ fm) [26, 43]		
Eskola *et al.*	900	3100
($b = 0$) [44]	(Pb-Pb)	
HIJING+ZPC+ART	1100	
[95, 26]	($b = 0$)	
UrQMD	1100	
[40, 26]	($b \leq 3$ fm)	
VNI+UrQMD	1000	
[89, 26]	($b \leq 1$ fm)	
Hydro+UrQMD	750	
[92]	($b = 0$)	
VNI+HSD	1150	
[26]	($b \leq 2$ fm)	
VENUS 4.12		8400 ($dN/d\eta$ at $\eta = 0$,
[22]		$b \leq 3$ fm, $\sqrt{s} = 6$ TeV per nucleon)
NEXUS	1100	
[26]	($b < 2$ fm)	
Statistical	1550	7560
($5 \div 10$ %) [5, 101, 26]		
WA98 extrapolation	1000	2500
(maximum $dN/d\eta$, ~ 10 %) [56]	(Pb-Pb)	
WNM	560	1220
	($\overline{n}_{\rm A} = 190$)	($\overline{n}_{\rm A} = 200$)
Percolation	910	1980
($b = 0$)	(Pb-Pb)	

Table 3: Results obtained in the SFM [35] for charged particle production in different reactions, compared with the results for dN/dy at $y = 0$ in Au-Au at $\sqrt{s} = 200$ GeV per nucleon (910) and in Pb-Pb at $\sqrt{s} = 5.5$ TeV per nucleon (3140), with a degree of centrality of 5 %.

Reaction and observable	Result	Difference (%)
dN/dy at $y = 0$, Au-Au at $\sqrt{s} = 200$ GeV per nucleon, 5 % of centrality ($b \leq 3.2$ fm)	910	0
$dN/d\eta$ at $\eta = 0$, Au-Au at $\sqrt{s} = 200$ GeV per nucleon, 5 % of centrality ($b \leq 3.2$ fm)	730	−20
Maximum $dN/d\eta$, Au-Au at $\sqrt{s} = 200$ GeV per nucleon, 5 % of centrality ($b \leq 3.2$ fm)	770	−15
dN/dy at $y = 0$, Au-Au at $\sqrt{s} = 200$ GeV per nucleon, $b = 0$	1030	+13
dN/dy at $y = 0$, Pb-Pb at $\sqrt{s} = 200$ GeV per nucleon, $b \leq 3.2$ fm	960	+5
dN/dy at $y = 0$, Pb-Pb at $\sqrt{s} = 5.5$ TeV per nucleon, 5 % of centrality ($b \leq 3.3$ fm)	3140	0
$dN/d\eta$ at $\eta = 0$, Pb-Pb at $\sqrt{s} = 5.5$ TeV per nucleon, 5 % of centrality ($b \leq 3.3$ fm)	2620	−17
Maximum $dN/d\eta$, Pb-Pb at $\sqrt{s} = 5.5$ TeV per nucleon, 5 % of centrality ($b \leq 3.3$ fm)	2820	−10
dN/dy at $y = 0$, Pb-Pb at $\sqrt{s} = 5.5$ TeV per nucleon, $b = 0$	3590	+14
dN/dy at $y = 0$, Pb-Pb at $\sqrt{s} = 7$ TeV per nucleon, 5 % of centrality ($b \leq 3.3$ fm)	3330	+6

commented at the end of Section 4, is the formation of color ropes with a large probability, which is required in the model to describe antibaryon enhancement at SPS because a rather large baryon-antibaryon annihilation cross section is used. In SFM, which considers a similar mechanism (string fusion), the charged density obtained is larger. The low value also obtained in Hydro+UrQMD is due to the initial QGP state and the first order transition assumed.

At LHC the differences among the predictions are larger, more than a factor 3. They lie in the range $2500 \div 8500$. Comparing Table 2 with Fig. 1, which summarizes the situation before 1996, it can be seen that nowadays predictions tend to gather around the lowest values; at the time of [22] only SFM gave predictions below 4000.

Essentially, models based on parton shower evolution predict larger values. Also statistical models obtain very large charged densities. However, the model described in Section 6, which uses mainly partonic degrees of freedom, obtains a low value (3100). This is due to the saturation of minijet production, which plays the role of an upper cut-off in the number of minijets. This saturation is a consequence of unitarity [48].

Unitarity is a basic ingredient that controls the number of soft and hard elementary scatterings (which are no more independent one from each other) in models like DPM, DPMJET, SFM and RQMD. In addition to that, energy-momentum conservation reduces the possible number of scatterings. Finally, interaction among strings is another collective effect which reduces central pion densities. In DPM these interactions are taken into account by means of the triple Pomeron. Its coupling is fixed to describe soft diffraction and HERA data. In other models as RQMD or SFM the interactions among strings are taken into account via the formation of color ropes or fusion of strings. Its strength is essentially fixed to reproduce heavy flavor and antibaryon enhancement at SPS. It is not unexpected that these three different forms of quantifying the shadowing give rise to similar predictions for global and simple observables as central rapidity densities of charged particles. Probably the knowledge of shadowing from small x physics can help to reconcile models based on partonic degrees of freedom with those based on strings as degrees of freedom. On the other hand, statistical thermal models predict a larger value close to 8000 as a consequence of the rather large volume at freeze-out. A reduction in a factor 3 would mean a strong reduction in this volume and a large change of the ratio between different particles, or in the temperature and chemical potential values.

In the summary talks of three mayor conferences [4, 5, 115] were quoted 8000, 8000, and between 3000 and 8000, for the probable number of charged particles per unit rapidity at the center of mass in central Pb-Pb collisions at the LHC. Models with interaction among strings obtain a lower value. The interplay between soft and hard physics is one of the main issues in the study of strong interactions and, together with the search and characterization

of QGP, one of the main goals of Heavy Ion Physics. Doubtless, the new experiments at RHIC and LHC will shed light on this subject, even measuring such a simple observable as central rapidity densities of charged particles.

Acknowledgements

This work has been done under contract AEN99-0589-C02 of CICYT (Spain). We express our gratitude to N. S. Amelin, M. A. Braun, A. Capella, W. Cassing, K. J. Eskola, E. G. Ferreiro, A. B. Kaidalov, J. Ranft, C. A. Salgado, H. Sorge, D. Sousa and K. Werner for useful discussions and comments.

References

[1] *Quark–Gluon Plasma*, ed. R. C. Hwa (World Scientific, Singapore, 1990); *Quark–Gluon Plasma 2*, ed. R. C. Hwa (World Scientific, Singapore, 1995).

[2] C.-Y. Wong, *Introduction to High-Energy Heavy-Ion Collisions* (World Scientific, Singapore, 1994); L. P. Csernai, *Introduction to Relativistic Heavy-Ion Collisions* (John Wiley & Sons, Chichester, 1994).

[3] J.-P. Blaizot, in *Proceedings of Quark Matter 99* (Torino, Italy, May 10th-15th 1999), to appear in *Nucl. Phys.* A (hep-ph/9909434, 1999).

[4] P. Braun-Munzinger, in *Proceedings of Quark Matter 99* (Torino, Italy, May 10th-15th 1999), to appear in *Nucl. Phys.* A (nucl-ex/9908007, 1999).

[5] J. Stachel, in *Proceedings of the XXIX International Symposium on Multiparticle Dynamics* (Providence, USA, August 9th-13th 1999), to be published by World Scientific.

[6] C. Pajares, *Acta Physica Polonica* B30 (1999) 2263.

[7] T. Matsui and H. Satz, *Phys. Lett.* B178 (1986) 416.

[8] J. Rafelski and B. Müller, *Phys. Rev. Lett.* 48 (1982) 1066; Erratum: *ibid.* 56 (1986) 2334.

[9] J. Rafelski, *Phys. Rep.* 88 (1982) 331.

[10] NA50 Collaboration: M. C. Abreu *et al.*, *Phys. Lett.* B410 (1997) 327; *ibid.* 337.

[11] WA97 Collaboration: E. Andersen *et al.*, *Phys. Lett.* B433 (1998) 209; NA49 Collaboration: H. Appelshauser *et al.*, *ibid.* B444 (1998) 523; WA85 Collaboration: F. Antinori *et al.*, *ibid.* B447 (1999) 178.

[12] CERES Collaboration: G. Agakichiev *et al.*, *Phys. Rev. Lett.* 75 (1995) 1272; *Phys. Lett.* B422 (1998) 405.

[13] J.-P. Blaizot and J.-Y. Ollitrault, *Phys. Rev. Lett.* 77 (1996) 1703.

[14] C.-Y. Wong, *Phys. Rev.* C55 (1997) 2621.

[15] D. Kharzeev, M. Nardi and H. Satz, *Z. Phys.* C74 (1997) 307.

[16] N. Armesto, M. A. Braun, E. G. Ferreiro and C. Pajares, *Phys. Rev. Lett.* 77 (1996) 3736.

[17] N. Armesto, A. Capella and E. G. Ferreiro, *Phys. Rev.* C59 (1999) 395.

[18] J. Geiss, C. Greiner, E. L. Bratkovskaya, W. Cassing and U. Mosel, *Phys. Lett.* B447 (1999) 31.

[19] S. E. Vance, M. Gyulassy and X.-N. Wang, *Phys. Lett.* B443 (1998) 45.

[20] A. Capella, E. G. Ferreiro and C. A. Salgado, *Phys. Lett.* B459 (1999) 27.

[21] G. Q. Li, C. M. Ko and G. E. Brown, *Phys. Rev. Lett.* 75 (1995) 4007.

[22] ALICE Collaboration: *Technical Proposal for A Large Ion Collider Experiment at the CERN LHC*, preprint CERN/LHCC/95-71 (1995).

[23] N. S. Amelin, M. A. Braun and C. Pajares, *Phys. Lett.* B306 (1993) 312; *Z. Phys.* C63 (1994) 507.

[24] K. Werner, *Phys. Rep.* 232 (1993) 87.

[25] N. van Eijndhoven *et al.*, Internal Note ALICE 95-32 (1995).

[26] S. A. Bass *et al.*, *Last Call for RHIC Predictions*, in *Proceedings of Quark Matter 99* (Torino, Italy, May 10th-15th 1999), to appear in *Nucl. Phys.* A (nucl-th/9907090, 1999).

[27] A. Capella, U. P. Sukhatme, C.-I. Tan and J. Tran Thanh Van, *Phys. Lett.* 81B (1979) 69; *Phys. Rep.* 236 (1994) 225; A. Capella, preprint LPT-Orsay 99-75 (hep-ph/9910219, 1999).

[28] A. Capella, J. Kwiecinski and J. Tran Thanh Van, *Phys. Lett.* B108 (1982) 347.

[29] A. Capella, C. Pajares and A. V. Ramallo, *Nucl. Phys.* B241 (1984) 75.

[30] J. Ranft, *Phys. Rev.* D51 (1995) 64.

[31] J. Ranft, preprint SI-99-5 (hep-ph/9911213, 1999).

[32] A. B. Kaidalov and K. A. Ter-Martirosyan, *Phys. Lett.* B117 (1982) 247.

[33] B. Andersson, G. Gustafson and B. Nilsson-Almqvist, *Nucl. Phys.* B281 (1987) 289; B. Nilsson-Almqvist and E. Stenlund, *Comput. Phys. Commun.* 43 (1987) 387.

[34] N. S. Amelin, L. V. Bravina, L. P. Csernai, V. D. Toneev, K. K. Gudima and S. Yu. Sivoklokov, *Phys. Rev.* C47 (1993) 2299.

[35] N. S. Amelin, N. Armesto, C. Pajares and D. Sousa, in preparation.

[36] H. Sorge, H. Stöcker and W. Greiner, *Ann. Phys.* 192 (1989) 266.

[37] H. Sorge, M. Berenguer, H. Stöcker and W. Greiner, *Phys. Lett.* B289 (1992) 6.

[38] H. Sorge, *Phys. Rev.* C52 (1995) 3291.

[39] M. Bleicher *et al.*, *J. Phys.* G25 (1999) 1859.

[40] M. Bleicher, S. A. Bass, H. Stöcker and W. Greiner, in *Proceedings of Quark Matter 99* (Torino, Italy, May 10th-15th 1999), to appear in *Nucl. Phys.* A (hep-ph/9906398, 1999).

[41] M. Hladik, PhD. Thesis, Nantes, December 1999; H. J. Drescher, M. Hladik, S. Ostapchenko and K. Werner, *J. Phys.* G25 (1999) L91; in *Proceedings of Quark Matter 99* (Torino, Italy, May 10th-15th 1999), to appear in *Nucl. Phys.* A (hep-ph/9906428, 1999).

[42] A. Tai, preprint LU-TP-94-22; preprint LU-TP-95-2; B.-H. Sa, Z.-Q. Wang, X.-Z. Zhang, G. Song, Z.-D. Lu and Y.-M. Zheng, *Phys. Rev.* C48 (1993) 2995; B.-H. Sa, A. Tai and Z.-D. Lu, *Phys. Rev.* C52 (1995) 2069; B.-H. Sa and A. Tai, *Phys. Rev.* C55 (1997) 2010; C57 (1998) 261.

[43] X.-N. Wang and M. Gyulassy, *Phys. Rev.* D44 (1991) 3501; D45 (1992) 844; M. Gyulassy and X.-N. Wang, *Comput. Phys. Commun.* 83 (1994) 307; X.-N. Wang, in *Proceedings of Quark Matter 99* (Torino, Italy, May 10th-15th 1999), to appear in *Nucl. Phys.* A (nucl-th/9907093, 1999).

[44] K. J. Eskola and K. Kajantie, *Z. Phys.* C75 (1997) 515; K. J. Eskola, *Comments Nucl. Part. Phys.* 22 (1998) 185; K. J. Eskola, K. Kajantie, P. V. Ruuskanen and K. Tuominen, preprint JYFL-8-99 (hep-ph/9909456, 1999); K. J. Eskola and K. Tuominen, in *Proceedings of Quark Matter 99* (Torino, Italy, May 10th-15th 1999), to appear in *Nucl. Phys.* A (hep-ph/9906438, 1999).

[45] K. Geiger and B. Müller, *Nucl. Phys.* B369 (1992) 600; K. Geiger, *Phys. Rev.* D47 (1993) 133.

[46] J.-P. Blaizot and A. H. Mueller, *Nucl. Phys.* B289 (1987) 847; K. Kajantie, P. V. Landshoff and J. Lindfors, *Phys. Rev. Lett.* 59 (1987) 2527.

[47] K. Kajantie, in *Proceedings of the 15th International Conference on Particle and Nuclei (PANIC 99)* (Uppsala, Sweden, June 10th-16th 1999), hep-ph/9907544 (1999).

[48] A. H. Mueller, *Nucl. Phys.* A654 (1999) 37; preprint CU-TP-937 (hep-ph/9904404, 1999); preprint CU-TP-954 (hep-ph/9911289, 1999).

[49] G. 't Hooft, *Nucl. Phys.* B72 (1974) 461; G. Veneziano, *Nucl. Phys.* B74 (1974) 365.

[50] V. N. Gribov, *Sov. Phys. JETP* 26 (1968) 414.

[51] R. J. Glauber, in *Lectures in Theoretical Physics*, Vol. 1, ed. W. E. Brittin and L. G. Duham (Interscience, New York, 1959).

[52] V. N. Gribov, *Sov. Phys. JETP* 29 (1969) 483; *ibid.* 30 (1970) 709.

[53] A. Bialas, M. Bleszyński and W. Czyz, *Nucl. Phys.* B111 (1976) 461.

[54] A. Bialas, in *Proceedings of the XIIIth International Symposium on Multiparticle Dynamics*, ed. W. Kittel, W. Metzger and A. Stergiou (World Scientific, Singapore, 1983).

[55] NA49 Collaboration: F. Siklér *et al.*, in *Proceedings of Quark Matter 99* (Torino, Italy, May 10th-15th 1999), to appear in *Nucl. Phys.* A; NA35 Collaboration: T. Alber *et al.*, preprint IKF-HENPG/6-94 (1997); M. Gaździcki and D. Röhrich, *Z. Phys.* C65 (1995) 215.

[56] WA98 Collaboration: T. Peitzmann *et al.*, in *Proceedings of Quark Matter 99* (Torino, Italy, May 10th-15th 1999), to appear in *Nucl. Phys.* A.

[57] A. Capella, C. Merino and J. Tran Thanh Van, *Phys. Lett.* B265 (1991) 415.

[58] A. Capella, A. B. Kaidalov and J. Tran Thanh Van, *Heavy Ion Physics* 9 (1999) 169.

[59] A. Capella, A. B. Kaidalov, C. Merino, D. Pertermann and J. Tran Thanh Van, *Phys. Rev.* D53 (1996) 2309; *Eur. Phys. J.* C5 (1998) 111.

[60] A. Capella, J. Kwiecinski and J. Tran Thanh Van, *Phys. Rev. Lett.* 58 (1987) 2015.

[61] T. Sjöstrand and M. van Zijl, *Phys. Rev.* D36 (1987) 2019.

[62] H.-U. Bengtsson and T. Sjöstrand, *Comput. Phys. Commun.* 46 (1987) 43.

[63] M. Glück, E. Reya and A. Vogt, *Eur. Phys. J.* C5 (1998) 461.

[64] A. Capella and B. Z. Kopeliovich, *Phys. Lett.* B381 (1996) 325; A. Capella and C. A. Salgado, *Phys. Rev.* C60 (1999) 054906.

[65] S. E. Vance and M. Gyulassy, *Phys. Rev. Lett.* 83 (1999) 1735; D. Kharzeev, *Phys. Lett.* B378 (1996) 238; B. Z. Kopeliovich and B. Povh, *Phys. Lett.* B446 (1999) 321; J. A. Casado, *Nucl. Phys.* A651 (1999) 93.

[66] G. C. Rossi and G. Veneziano, *Nucl. Phys.* B123 (1977) 507.

[67] D. J. Gross and H. Ooguri, *Phys. Rev.* D58 (1998) 106002.

[68] M. A. Braun and C. Pajares, *Phys. Lett.* B287 (1992) 154; *Nucl. Phys.* B390 (1993) 542; *ibid.* 559.

[69] C. Merino, C. Pajares and J. Ranft, *Phys. Lett.* B276 (1992) 168; H. J. Möhring, J. Ranft, C. Merino and C. Pajares, *Phys. Rev.* D47 (1993) 4142.

[70] J. Schwinger, *Phys. Rev.* 82 (1951) 664.

[71] A. Casher, H. Neuberger and S. Nussinov, *Phys. Rev.* D20 (1979) 179.

[72] T. S. Biró, H. B. Nielsen and J. Knoll, *Nucl. Phys.* B245 (1984) 449.

[73] B. Andersson and P. A. Henning, *Nucl. Phys.* B355 (1991) 82.

[74] M. Nardi and H. Satz, *Phys. Lett.* B442 (1998) 14; H. Satz, *Nucl. Phys.* A642 (1998) 130.

[75] M. A. Braun, C. Pajares and J. Ranft, *Int. J. Mod. Phys.* A14 (1999) 2689.

[76] N. Armesto, M. A. Braun, E. G. Ferreiro and C. Pajares, in *Proceedings of Quark Matter 99* (Torino, Italy, May 10th-15th 1999), to appear in *Nucl. Phys.* A; M. A. Braun and C. Pajares, preprint US-FT-15-99 (hep-ph/9907332, 1999), to appear in *Eur. Phys. J.* C.

[77] N. Armesto, M. A. Braun, E. G. Ferreiro, C. Pajares and Yu. M. Shabelski, *Phys. Lett.* B389 (1996) 78; *Astropart. Phys.* 6 (1997) 327.

[78] N. Armesto, M. A. Braun, E. G. Ferreiro and C. Pajares, *Phys. Lett.* B344 (1995) 301.

[79] E. V. Shuryak, hep-ph/9911244 (1999); *Phys. Lett.* 79B (1978) 135.

[80] G. S. Bali, preprint HUB-EP-98-57 (hep-ph/9809351, 1998); F. V. Gubarev, E. M. Ilgenfritz, M .I. Polikarpov and T. Suzuki, preprint ITEP-TH-43-99 (hep-lat/9909099, 1999).

[81] B. Andersson, G. Gustafson, G. Ingelman and T. Sjöstrand, *Phys. Rep.* 97 (1983) 31; T. Sjöstrand, *Comput. Phys. Commun.* 39 (1986) 347.

[82] H. Sorge, in *Proceedings of Quark Matter 99* (Torino, Italy, May 10th-15th 1999), to appear in *Nucl. Phys.* A (nucl-th/9906051, 1999).

[83] X.-N. Wang, *Phys. Rev.* C58 (1998) 2321; X.-N. Wang and M. Gyulassy, *Phys. Rev. Lett.* 68 (1992) 1480.

[84] K. J. Eskola, V. J. Kolhinen and C. A. Salgado, *Eur. Phys. J.* C9 (1999) 61.

[85] L. McLerran and R. Venugopalan, *Phys. Rev.* D49 (1994) 2233; *ibid.* 3352; *ibid.* D50 (1994) 2225; L. McLerran, preprint TPI-MINN-99-14 (hep-ph/9903536, 1999).

[86] A. Krasnitz and R. Venugopalan, in *Proceedings of the XXIX International Symposium on Multiparticle Dynamics* (Providence, USA, August 9th-13th 1999), to be published by World Scientific (hep-ph/9910391, 1999); hep-ph/9909203 (1999).

[87] K. Werner and J. Aichelin, *Phys. Rev. Lett.* 76 (1996) 1027.

[88] B. Andersson, *Phys. Lett.* B256 (1991) 337.

[89] S. A. Bass, M. Hofmann, M. Bleicher, L. V. Bravina, E. E. Zabrodin, H. Stöcker and W. Greiner, *Phys. Rev.* C60 (1999) 021901.

[90] K. Geiger, *Comput. Phys. Commun.* 104 (1997) 70.

[91] S. A. Bass and B. Müller, preprint DUKE-TH-99-192 (nucl-th/9908014, 1999), to appear in *Phys. Lett.* B.

[92] S. A. Bass, A. Dumitru, M. Bleicher, L. V. Bravina, E. E. Zabrodin, H. Stöcker and W. Greiner, *Phys. Rev.* C60 (1999) 021902.

[93] W. Cassing, E. L. Bratkovskaya, J. Geiss, C. Greiner, S. Juchem and U. Mosel, in *Proceedings of Quark Matter 99* (Torino, Italy, May 10th-15th 1999), to appear in *Nucl. Phys.* A (nucl-th/9906072, 1999).

[94] W. Cassing and E. L. Bratkovskaya, *Phys. Rep.* 308 (1999) 65; *Nucl. Phys.* A623 (1997) 570.

[95] B. Zhang, C. M. Ko, B.-A. Li and Z. Lin, nucl-th/9904075 (1999).

[96] B. Zhang, *Comput. Phys. Commun.* 109 (1998) 193.

[97] B.-A. Li and C. M. Ko, *Phys. Rev.* C52 (1995) 2037.

[98] J. Sollfrank and U. Heinz, in *Quark–Gluon Plasma 2*, ed. R. C. Hwa (World Scientific, Singapore, 1995).

[99] F. Becattini and U. Heinz, *Z. Phys.* C76 (1997) 269.

[100] J. Cleymans and K. Redlich, *Phys. Rev. Lett.* 81 (1998) 5284.

[101] P. Braun-Munzinger, I. Heppe and J. Stachel, *Phys. Lett.* B465 (1999) 15.

[102] E. E. Zabrodin, L. V. Bravina, H. Stöcker and W. Greiner, hep-ph/9901356 (1999).

[103] E. Fermi, *Prog. Theor. Phys.* 5 (1950) 570; *Phys. Rev.* 81 (1951) 683.

[104] L. D. Landau, *Izv. Akad. Nauk Ser. Fiz.* 17 (1953) 51; S. Z. Belenkij and L. D. Landau, *Nuovo Cim. Suppl.* 3 (1956) 15; I. J. Pomeranchuk, *Dokl. Akad. Nauk Ser. Fiz.* 78 (1951) 889.

[105] R. Hagedorn, *Nuovo Cim. Suppl.* 3 (1965) 147.

[106] T. S. Biró, P. Lévai and J. Zimányi, *Phys. Rev.* C59 (1999) 1574; J. Zimányi, T. S. Biró, T. Csörgö and P. Lévai, hep-ph/9904501 (1999).

[107] H. Satz, in *Proceedings of Quark Matter 99* (Torino, Italy, May 10th-15th 1999), to appear in *Nucl. Phys.* A (hep-ph/9908339, 1999).

[108] M. B. Isichenko, *Rev. Mod. Phys.* 64 (1992) 961; D. Stauffer and A. Aharony, *Introduction to Percolation Theory* (Taylor & Francis, London, 1994).

[109] J. Dias de Deus, R. Ugoccioni and A. Rodrigues, preprint FISIST-10-99-CENTRA (hep-ph/9907352, 1999).

[110] G. Baym, *Physica* 96A (1979) 131; T. Celik, F. Karsch and H. Satz, *Phys. Lett.* B97 (1980) 128.

[111] T. K. Gaisser, *Cosmic Rays and Particle Physics* (Cambridge University Press, Cambridge, 1991).

[112] C. Pajares, D. Sousa and R. A. Vázquez, hep-ph/9805475 (1998), to appear in *Astropart. Phys.*

[113] G. Battistoni, C. Forti, J. Ranft and S. Roesler, *Astropart. Phys.* 7 (1997) 49; G. Battistoni, M. Carboni, C. Forti and J. Ranft, preprint INFN-AE-99-07 (1999).

[114] D. Heck, G. Schatz, T. Thouw, J. Knapp and J. N. Capdevielle, preprint FZKA-6019 (1998); D. Heck and J. Knapp, preprint FZKA-6097 (1998).

[115] K. J. Eskola, in *Proceedings of the International Europhysics Conference on High Energy Physics* (Tampere, Finland, July 15th-21st 1999), to be published by IOP Publishing (hep-ph/9911350, 1999).

FIGURES

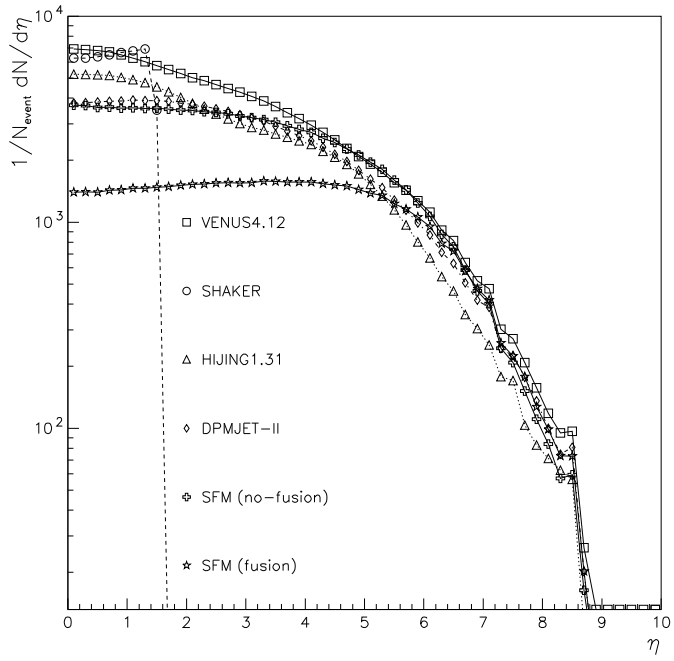

Figure 1: Predictions from different models for the charged pseudorapidity density in central ($b \leq 3$ fm) Pb-Pb collisions at the LHC, taken from [22].

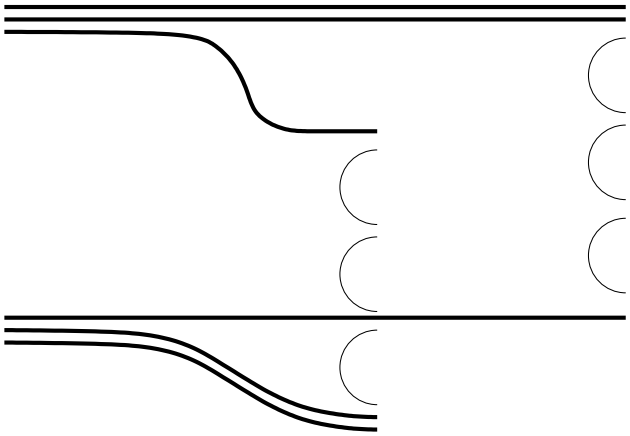

Figure 2: Lowest order contribution to p-p scattering at high energies in the DPM. Strings are stretched between valence constituents of the protons and hadronize by means of $q\overline{q}$ pair production.

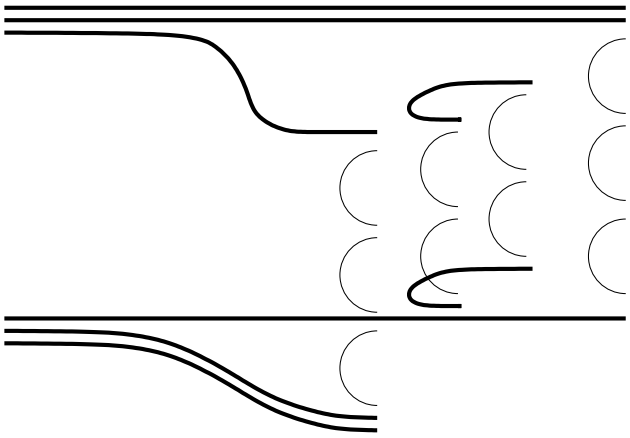

Figure 3: First higher order contribution to p-p scattering at high energies in the DPM. Besides the contribution shown in Fig. 2, now strings stretched between sea constituents of the protons appear.

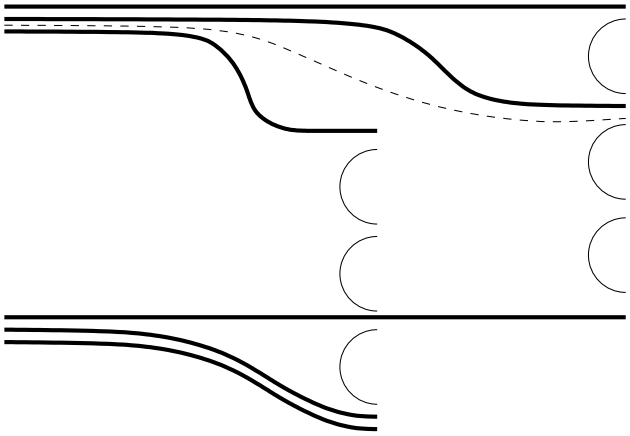

Figure 4: The popcorn mechanism of diquark breaking.

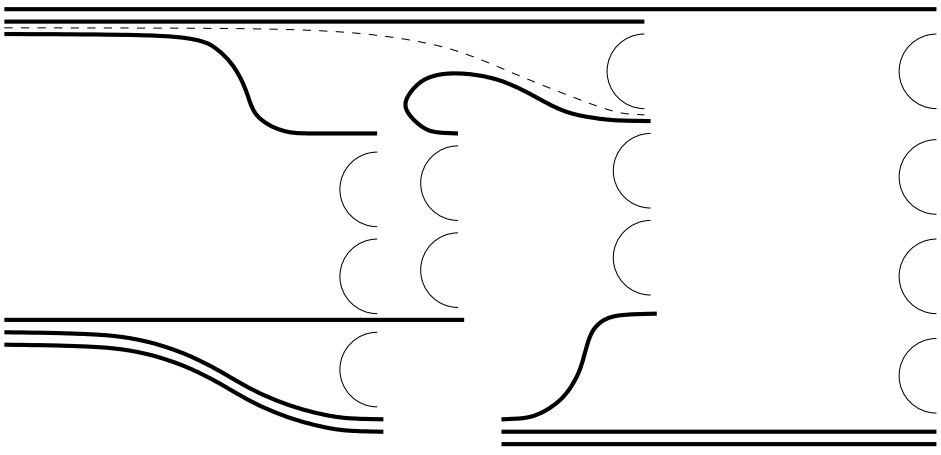

Figure 5: One example of proposed diagram for diquark breaking in nucleon-nucleus collisions.

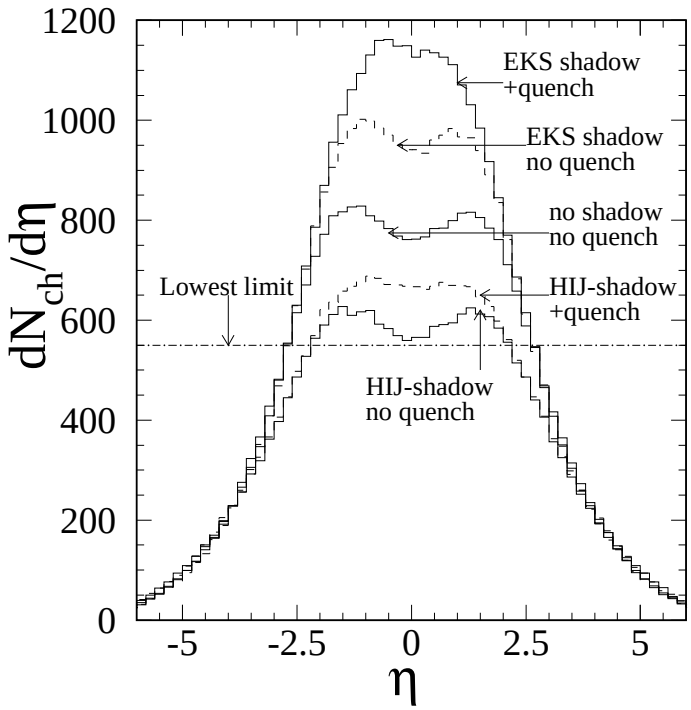

Figure 6: Predictions for the charged pseudorapidity density in central ($b < 3$ fm) Au-Au collisions at RHIC in the HIJING model, taken from [26].

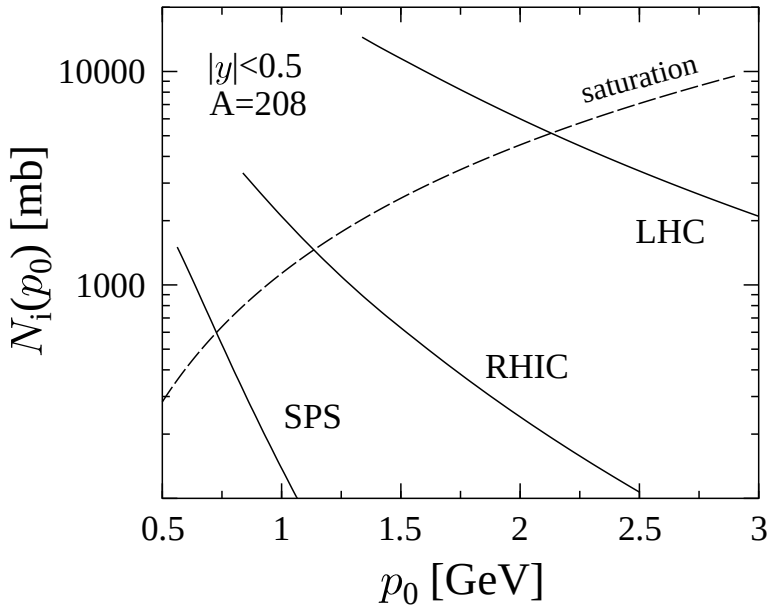

Figure 7: $N_{\rm AA}(b=0,p_0,\sqrt{s})$ with $p_T \geq p_0$ and $|y| < 0.5$ for A = 208 as a function of p_0 at $\sqrt{s} = 5500$ (LHC), 200 (RHIC) and 17 (SPS) GeV per nucleon, taken from [44]. The dashed curve is $p_0^2 R_{\rm A}^2$.

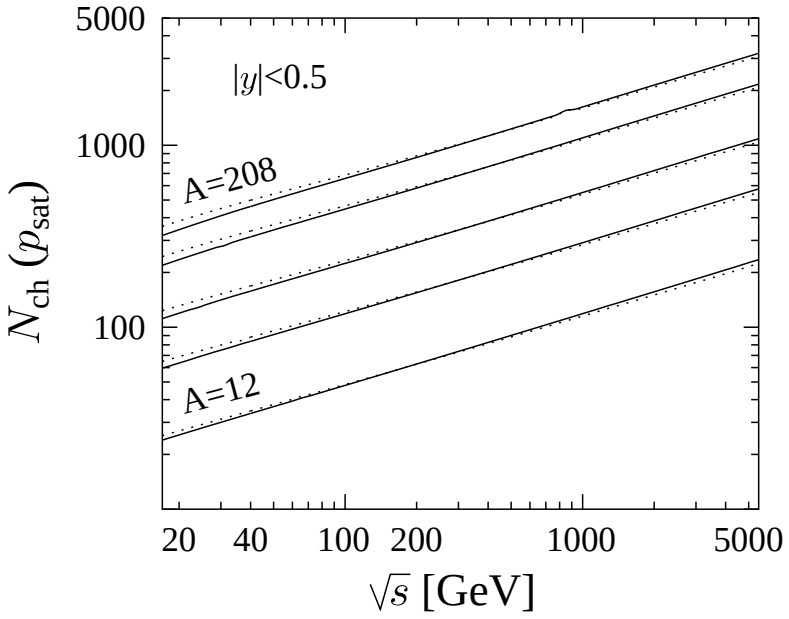

Figure 8: Rapidity density of charged particles at $y = 0$ for A = 12, 32, 64, 136 and 208 as a function of $\sqrt{s}$ for central A-A collisions, taken from [44]. The dotted line is the result of (27), the solid line is the result of a more rigorous calculation.

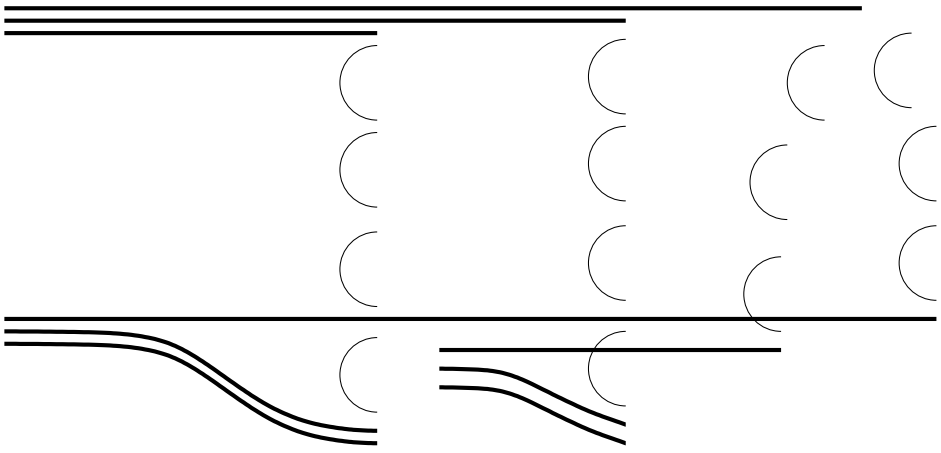

Figure 9: Example of diagram with two color exchanges in VENUS.

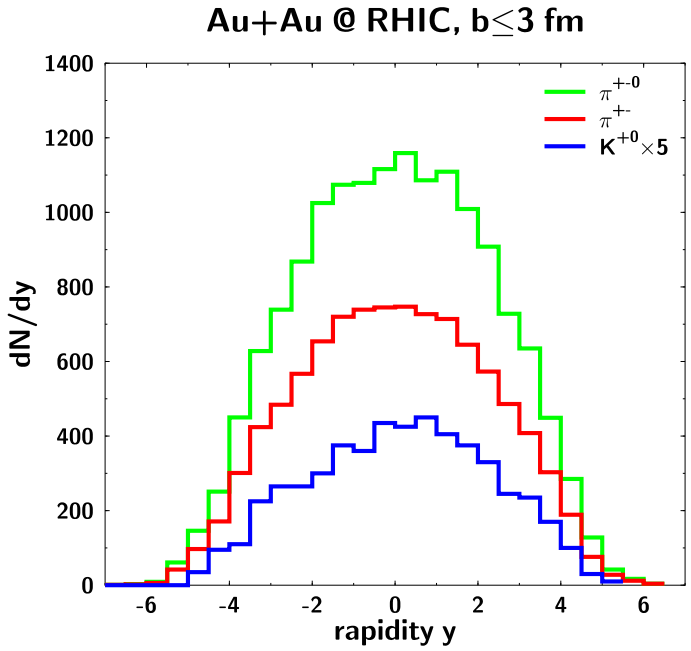

Figure 10: Predictions for the charged rapidity density in central ($b \leq 3$ fm) Au-Au collisions at RHIC in the UrQMD model, taken from [40, 26].

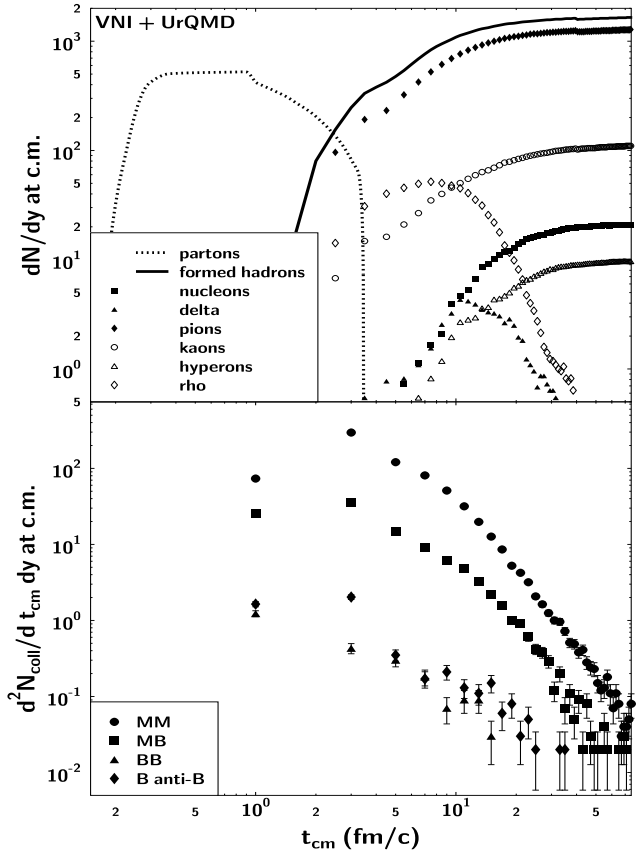

Figure 11: Time evolution of parton and on-shell hadron rapidity densities for central ($b \leq 1$ fm) at RHIC in the VNI+UrQMD model, taken from [89, 26].

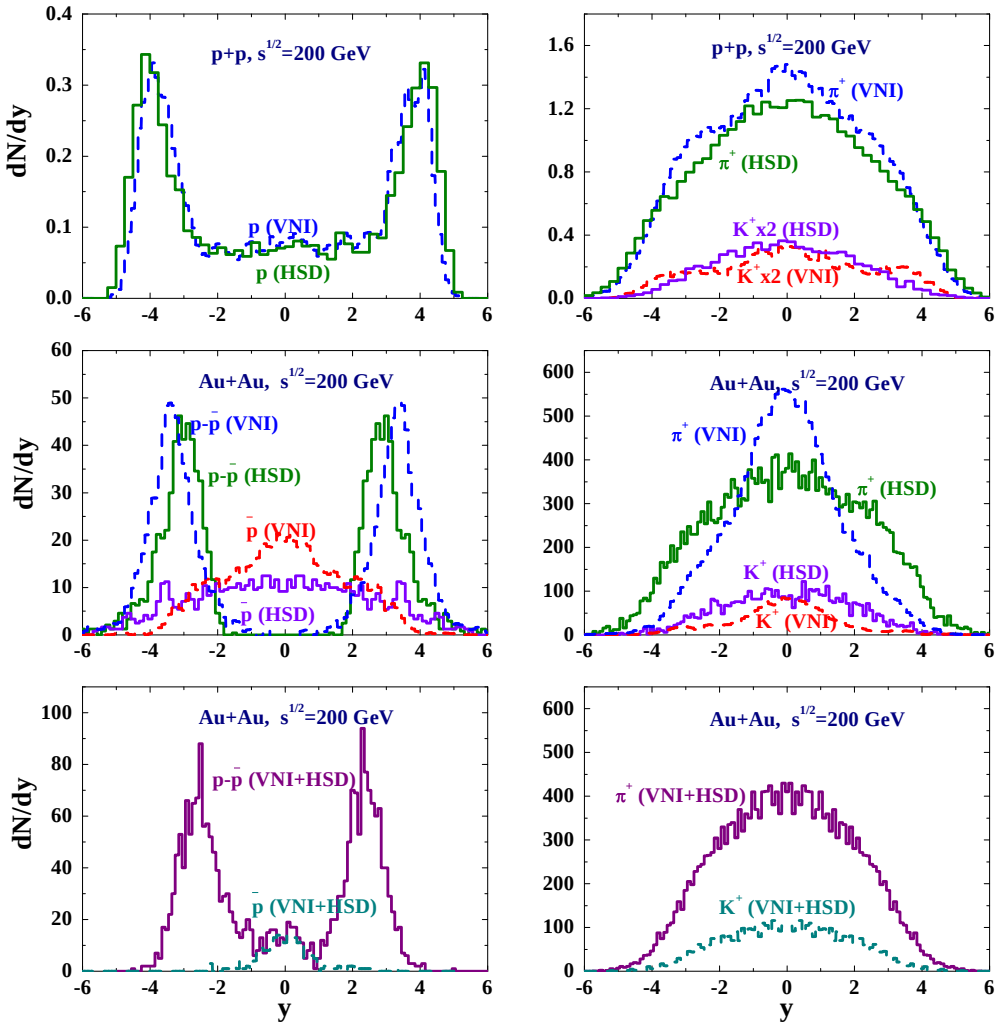

Figure 12: Predictions for rapidity distributions of several particles in p-p and central ($b \leq 2$ fm) Au-Au collisions at RHIC from VNI, HSD and VNI+HSD models, taken from [26].